Green Synthesis of Lidocaine Ionic Liquids and Salts: Mechanisms of Formation and Interactions in the Crystalline and Supercooled States

Julija Zotova[1]; Zaneta Wojnarowska[2]; Brendan Twamley[3]; Marian Paluch[2]; Lidia Tajber[1]*

[1] School of Pharmacy and Pharmaceutical Sciences, Trinity College Dublin, College Green, Dublin 2, Ireland

[2] Institute of Physics, University of Silesia, SMCEBI, 75 Pulku Piechoty 1A, 41-500 Chorzow, Poland

[3] School of Chemistry, Trinity College Dublin, College Green, Dublin 2, Ireland

* Corresponding author, Lidia Tajber, School of Pharmacy and Pharmaceutical Sciences, Trinity College Dublin, College Green, Dublin 2, Ireland. Tel: +35318962787. Email: ltajber@tcd.ie

Abstract

Mechanochemistry has been recognised as an optimal route for the synthesis of ionic liquids incorporating active pharmaceutical ingredients (API-ILs) as it eliminates the need for large volumes of solvents and purification steps, thus making it a sustainable alternative to conventional solution synthesis. In this work a range of API-ILs incorporating lidocaine and medium-chain dicarboxylic acids as the counterions were synthesised by neat grinding and the effect of an alkyl chain length on the phase formation was investigated. The evaluation of thermal and dynamic behaviours as well as crystallographic analysis of API-ILs was performed in an attempt to devise a prediction tool for structure-property relationship. Alternating trends in morphology, melting points, glass transition temperatures and crystallographic properties of the new phases were observed across the dicarboxylic acid series. This study enhanced our understanding of the mechanisms of API-ILs formation and contributed to the current aim of the ILs community to devise a systematic approach for API-IL discovery and development for pharmaceutical applications.

Keywords: lidocaine, active pharmaceutical ingredient (API), dicarboxylic acid, mechanochemistry, thermal analysis, ionisation, dielectric spectroscopy.

Introduction

One of the areas of pharmaceutical research that has seen a significant increase in interest lies in the optimisation of physical forms of active pharmaceutical ingredients (APIs).[1,2] By tuning the solid form of APIs it is possible to improve a drug's solubility, permeability and thus, bioavailability. As a result, a significant amount of research has led to the development of various multicomponent API systems, including crystalline salts, co-crystals, eutectics, deep eutectic mixtures, ionic liquids and solid dispersions.[3]

Purely ionic and purely neutral multicomponent systems are the two opposite extremes of a physical modification spectrum. Solid ionic salts constitute approximately 50% of currently marketed drug substances.[4] On the opposite end of the spectrum, neutral multicomponent systems, such as cocrystals, are in the spotlight of current research and a rapidly growing pharmaceutical form of choice.

One of the possible physical modifications that can achieve the balance between the desired physicochemical properties and maintenance (or even enhancement) of pharmacological function of APIs is low melting salts or ionic liquids (ILs). ILs are salts with melting points or glass transition temperatures below 100 °C.[5] In molten states the ions are not randomly distributed but form aggregates, clusters or regular 3D networks via intermolecular interactions. The advantage of employing ILs in pharmaceutical formulations is the ability to obtain highly tunable systems and simultaneously avoid polymorphic interconversions which are often encountered in solid forms.[6,7,8] Protic ionic liquids (PILs) are fused salts held together by partially-transferred labile protons and are often prepared by simple acid-base neutralisation reactions.

PILs can be prepared by a number of different methods, including conventional solution synthesis or by a simple mechanochemical technique. In most cases it involves milling, neat grinding or solvent-assisted grinding of chemical substances at ambient temperatures or with heating.[9] Neat mechanochemical synthesis initiates a series of mechanisms which include molecular diffusion, eutectic formation and crystallisation through an amorphous phase.[10] This technique eliminates the need for large volumes of solvents and lengthy conventional solution syntheses and it has been demonstrated that the products

prepared via mechanochemistry are obtained in higher yields, without solvent residues and in a shorter time span.[11] Over the years, ILs became renown as sustainable and green materials.[12,13]

Reactivity in crystals depends on a balance between steric packing factors and electronic properties and the fundamental problem is how the two processes are interrelated. Sufficient difference in pK_a values (i.e. $\Delta pK_a = pK_a(base) - pK_a(acid)$) allows ionisation to take place, however bulky molecular structures of the counterions do not allow the molecules to come into close contact hence inhibiting crystallisation. Identification of suitable counterions for API-PIL formation is a challenge currently faced and involves recognising certain structural characteristics, such as a diffuse delocalised charge, low symmetry and a low tendency of the counterion to crystallise.[14] Nevertheless, many attempts to correlate the structural considerations of the starting materials and the melting points of the synthesised salts have not provided an accurate prediction tool for IL formation.[15,16] Currently, an anti-crystal engineering approach is regarded as the most effective prediction method for IL formation.[17,18]

Over the last decade many different API-PIL and other multicomponent drug forms have been studied. Lidocaine (LID) has been one of the most widely studied APIs as a component in PILs. It is an aminoamide drug used as a local anaesthetic and cardiac depressant. It has also been shown to possess antibacterial[19] and antifungal[20] properties. However, when formulated as a salt its charge does not allow it to effectively penetrate biological membranes[21] and thus, significantly reduces its membrane permeability. By selecting a suitable counterion LID can be formulated as a protic ionic liquid system.

In this work, a green approach into the synthesis of multicomponent phases of lidocaine – dicarboxylic acid (LID:DA) systems was applied and the mechanism of the various phase formation studied to determine the effect of an alkyl chain length on the phase formation. Molecular structures of LID and DAs are shown in **Scheme 1**. The dicarboxylic acids chosen were medium chain dicarboxylic acids with carbon chain length ranging n=5-8 and their relevant physicochemical properties are presented in **Table S1**. In addition to meeting the physicochemical requirements, antifungal and antibacterial properties exhibited by some of the dicarboxylic acids render them suitable as potential companions for LID in topical formulations as dual API-ILs. [22]

Scheme 1. Chemical structures of the molecules investigated in this study: lidocaine base (LID); dicarboxylic acids (DA), where *n* is the number of carbon atoms in the backbone. Orange: H-bond donor and acceptor; purple: H-bond acceptor; green: carboxylic acid groups.

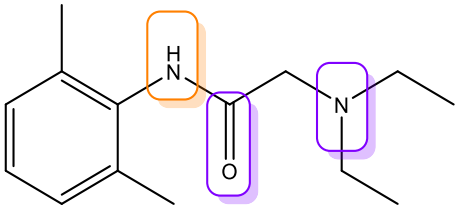

Lidocaine (LID)

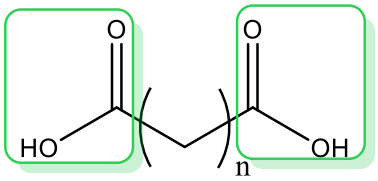

Dicarboxylic Acid (DA)

Results and discussion

Design strategy

Previously, short chain oxalic, malonic and succinic diacids have been probed as components for the LID:DA systems and it has been shown that molecular salts are formed through proton transfer from the dicarboxylic acids to the amine moiety on LID.[23] In the current study we took this concept further and aimed to synthesise new phases of LID with medium chain dicarboxylic acids. As a result of the increasing steric effect of the bulkier acids as well as employing a different synthetic method it was hypothesised that LID and DA can form interactions that are different to the ones reported in the Braga et al. work, where the LID-short DA systems were discussed. The effect of a synthetic method of choice on the formation of ionic or molecular species has been explored and emphasized previously.[24] Depending on the presence or absence of solvent, type of solvent and the choice of the reaction temperature, systems with different physical properties, molar ratios and species (e.g. ionic or molecular) could be obtained.

Alkyl dicarboxylic acids exhibit variation in their physicochemical properties based on the carbon chain length. Properties such as melting point, thermal expansion, solubility enthalpy, sublimation and crystal packing density alternate with the even or odd number of carbon atoms present in their backbone.[25,26,27] Lindemann proposed that crystalline structures which experience larger thermal expansion, exhibit lower melting points.[28] It has been shown that the diacids follow the Lindemann's correlation and

this alteration has been explained in terms of their packing and conformational distortion (**Figure 1A**). A static model from the 130K crystal structure data set for the C5-C8 diacids (i.e. glutaric (C5), adipic (C6), pimelic (C7) and suberic (C8) diacids) have shown that odd acids are more distorted from their equilibrium geometry to avoid unfavourable O…O repulsions, and that leads to lowering in melting point (**Figure 1B and 1C**).[25] This distortion and higher repulsion should make it easier to disrupt the crystal and form a new phase. In addition, in the range of even and odd diacids it is evident that longer chain lengths exhibit lower melting points.

The effects of these properties on the cocrystal formation have been studied before as in the examples of acid-amide heterosynthon systems.[29,30] A study on the formation of benzamide-DA derivatives has investigated the influence of the chain length on the formation of new phases when additional H-bond donors were competing in the heterosynthon formation.[16] In these examples it has been shown that even chain acids yield cocrystals with higher melting points and odd diacids yield cocrystals with lower melting points. In addition, systems with stronger intermolecular interactions (i.e. salts) exhibited a smallest decrease in the melting temperature as compared to the parent components, while systems with weaker interactions (i.e. cocrystals) exhibited significant drops in melting points.

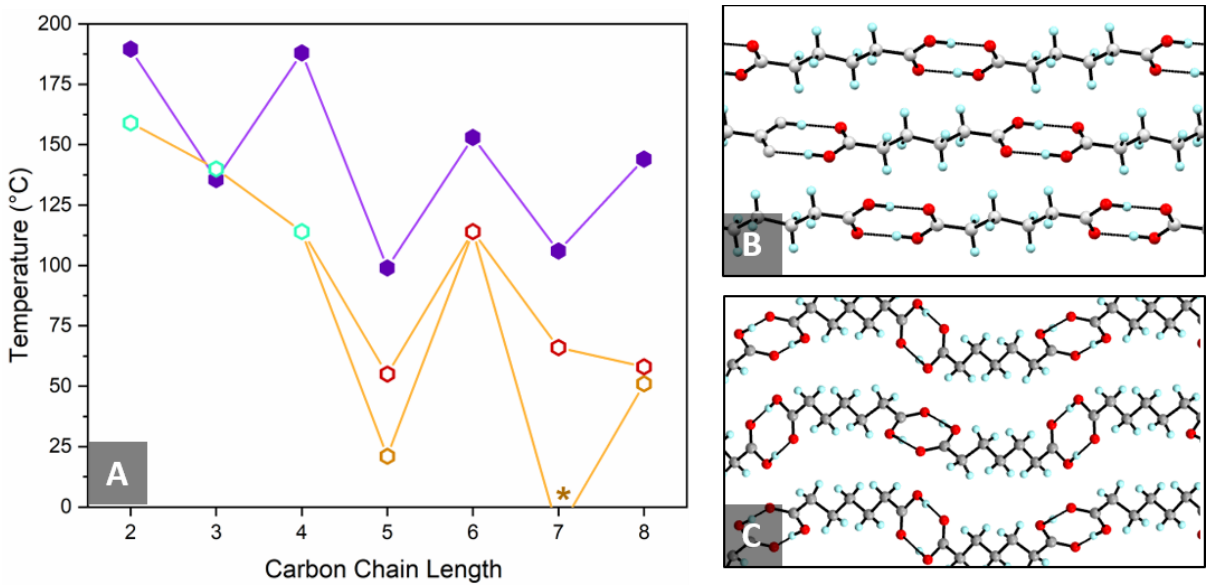

Figure 1. A: The melting points (purple symbols) for even and odd diacids alternate, with even diacids having higher melting points and odd diacids melting at lower temperatures. The experimental melting points (open symbols) obtained by DSC analysis for new LID:DA systems (orange symbols) show a similar alternating trend with the exception of LID:C4 (LID:succinic acid), which has a lower melting point than LID:C3 (LID:malonic acid). Data points for LID:C2 (LID:oxalic acid), LID:C3 and LID:C4 (green symbols) were obtained from literature.[23] The star indicates that the melting point could not be obtained as the sample is liquid above 0 °C. The red open symbols show the experimental melting points of the single crystals attained during the crystallographic studies. **B:** Crystal packing modes in even chain DAs as viewed along the *b*-axis; **C:** in odd chain diacids as viewed along the *a*-axis.

The API chosen to study the formation of multicomponent phases is lidocaine (LID) which is an amino-amide molecule with one H-bond donor and 3 H-bond acceptors. LID is a weak base (pK_a of 7.9) and all known LID salts undergo ionisation at the tertiary amine site.[23,31] In addition to the amine ionisation, LID can also engage in intermolecular H-bonding with carboxylic acids yielding acid-amide heterosynthons. In the case of non-ionised H-bonded complexes LID cocrystals or deep eutectic mixtures (DEMs) may be obtained.[32]

Mechanosynthesis of LID:DA systems and their morphologies

The study was initiated by solvent-free mechanochemical synthesis of the LID:DA systems. LID:C5 and LID:C7 systems with molar compositions that fall within $LID_{0.33}$:$DA_{0.67}$ and $LID_{0.67}$:$DA_{0.33}$ range yielded liquid or semiliquid samples at room temperature (**Figure S1**). On the contrary, LID:C6 and LID:C8 systems at all molar compositions were solid powders.

It was observed that upon physical contact LID and DAs demonstrate solid state reactivity. The crystals of the parent components were placed side by side and images obtained using Polarised Optical Microscopy (POM) illustrate that both, LID and DAs with C_{odd} (C5 and C7) undergo solid interdiffusion (**Figure 2**). The formation of a liquid eutectic as a product of a solid state reaction indicates that the melting point of the eutectic is lower than the reaction temperature, which in this case is room temperature. Inability to capture the melting point allows the term “deep eutectic” to be applied. LID and C8 display true solid

state reactivity with the formation of a solid eutectic at the interphase. LID and C6 underwent slight reactivity, probably initiated by the shear force resulting from sample handling with no further solid interdiffusion observed after t = 16 h.

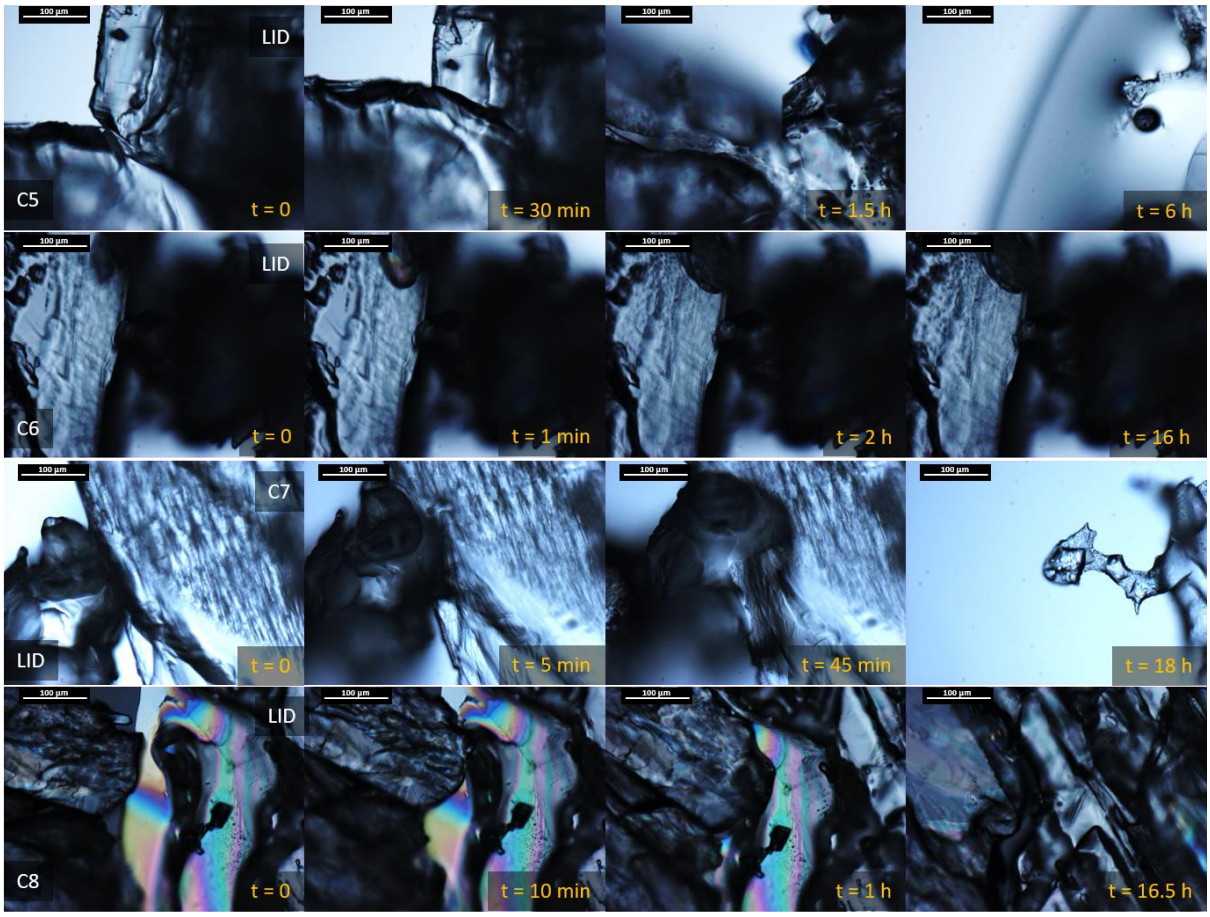

Figure 2. POM images of solid fusion experiments (at RT). The images were taken at various time points indicated by yellow font.

Mechanism of New Phase Formation and Thermodynamic Phase Diagrams

Differential Scanning Calorimetry (DSC) measurements were conducted to investigate thermal behaviour of LID, DAs and their binary mixtures. Stacks of DSC traces of the mixtures at different LID:DA molar ratios are presented in **Figure S2**. DSC thermogram of pure LID displays a single sharp endothermic peak at 69 °C corresponding to its melting transition. C5-C8 DAs have significantly higher melting points

ranging from 95 °C to 153 °C. Multiple endothermic peaks observed in the thermograms of pure C5 and C7 DAs are attributed to the multiple polymorphic forms, the stable β and metastable α forms (**Table S1**).[33,34] In addition, the peak at 85 °C in the pure C7 corresponds to the solid-solid order-disorder transition. A similar order-disorder transition is also observed in the pure C8 at 132 °C. Beta polymorphic forms of the odd acids are more stable and those were the ones found (by powder X-ray diffraction (PXRD), **Figure S2**) in precursor acids (DAs as supplied) used and also in most LID:DA samples after they were subjected to heating. Only upon heating of LID:C7 samples a peak in the PXRD pattern corresponding to the metastable α polymorph was identified. This peak is indicated by an arrow at 23 2θ degrees in **Figure S2g.**

The effect of the presence of DAs on LID was studied by observing its thermal behaviour in LID:DA binary mixtures at different molar ratios. Upon addition of an increasing molar fraction of C5 the melting point depression is observed (**Figure S2a**). The red arrow indicates the shift in the melting point until it gradually disappears due to complete solubilisation of LID within the LID:C5 liquid mixture. A similar melting point depression is observed for the C5 acid with increasing LID molar fraction. Eventually, in the range of $LID_{0.5}$:$C5_{0.5}$ to $LID_{0.2}$:$C5_{0.8}$ the melting points of the parent materials are depressed to the extent that the system liquefies and no melting events are observed. However, upon grinding the samples obtained were not homogenous liquids but contained white solid particles suspended in the liquid matrix. DSC analysis carried out at lower temperatures revealed endothermic peaks visible in thermograms of $LID_{0.33}$:$C5_{0.67}$ and $LID_{0.5}$:$C5_{0.5}$ samples below room temperature, at 21°C and 22°C, respectively. These new peaks can be attributed to a new phase formation, as later confirmed by PXRD analysis.

DSC traces of LID:C6 at a range of 0.1 to 1.0 LID molar fractions display an endothermic peak at 69 °C corresponding to the melting point of LID (**Figure S2b**). The lack of LID melting point depression corroborates POM images illustrating that mechanical grinding of LID and C6 does not initiate a solid state reaction. The thermograms of samples within $LID_{0.7}$:$C6_{0.3}$ and $LID_{0.4}$:$C6_{0.6}$ molar compositions reveal an exothermic event attributed to crystallisation with a peak temperature of 105 °C. Crystallisation is immediately followed by an endothermic peak with an onset temperature of 113 °C. The peak appears at a significantly higher temperature than the temperature of fusion of parent LID suggesting that the new phase

might be a new salt that has been formed upon reaction of molten LID with C6. Salt formation was later confirmed by PXRD and single crystal X-ray diffraction (SXRD) analysis. Upon addition of excess C6 the peak corresponding to the new phase gradually diminishes and is replaced by a eutectic peak at 105 °C which could possibly arise as a result of new interactions being formed between the new phase and the excess of C6. Pure C6 has a melting point at 148 °C but the melting point is depressed upon addition of increasing molar fractions of LID until eventually, at $LID_{0.3}$:$C6_{0.7}$ the peak completely disappears signifying that all of the acid is being used up in the formation of the new phase and the salt/acid eutectic.

The DSC thermograms of LID:C7 exhibit thermal behaviour similar to the one observed in the LID:C5 system. Liquefication of LID and C7 at room temperature reveals solid state reactivity and a deep eutectic formation between the new phase and excess parent components. The depression of LID and C7 melting points is observed as the molar fraction of the corresponding counterion in the binary mixtures is increased. Eventually, the melting points of the parent materials are depressed to the extent that the system liquefies and no melting events are observed. This observation is evident in the mixtures ranging from $LID_{0.6}$:$C7_{0.4}$ to $LID_{0.33}$:$C7_{0.67}$ molar ratios and is shown as green DSC traces in **Figure S2c**. Similar to LID:C5, upon grinding the samples obtained were not homogenous liquids but contained white solid particles suspended in the deep eutectic. However, attempts to capture the melting point of the new phase using DSC was not successful as upon heating the small crystals dispersed within a liquid matrix liquefied gradually and no endothermic peaks could not be observed. DSC scans of this sample when applying a heating rate of 300 K min^{-1} to prevent sample transformation, were also performed with an attempt to capture the melting points but these attempts were also unsuccessful.

Analogous to LID:C6, LID:C8 systems were solid in appearance. DSC thermal analysis revealed the formation of a new phase with a fusion temperature above RT at around 52 °C . Upon addition of excess C8 the formation of a new endothermic peak at 47 °C could be observed. This peak could be attributed to the fusion event of a eutectic formed between the new phase and the excess C8, as seen by POM (**Figure 2**).

Plotting the temperatures of the endothermic peaks of the new phases observed in all LID:DA systems displays a matching alternating trend as in the T_m of the parent DAs (**Figure 1**). This trend suggests that the melting points of the DAs used as the counterions in LID binary systems have a direct effect on the thermal behaviour of the API.

PXRD was used as the primary analytical method to identify new solid forms of LID with DAs. **Figure S2e** shows the diffraction patterns of LID:C5 systems. As $LID_{0.5}$:$C5_{0.5}$ and $LID_{0.33}$:$C5_{0.67}$ were obtained as liquid samples, the PXRD patterns at room temperature only exhibited typical liquid "halos". At higher LID molar fraction the PXRD pattern of $LID_{0.67}$:$C5_{0.33}$ sample revealed peaks originating from the excess LID in the mixture. As a result of the system being liquid at room temperature, it is not possible to conclude whether the samples are just physical mixtures or the interactions between the parent components give rise to the formation of a new phase. However, upon keeping the $LID_{0.5}$:$C5_{0.5}$ sample at 4 °C for a prolonged time, larger crystals phase-separated from the mixture. Thus, PXRD analysis confirmed new phase formation for the LID:C5 system. The melting point of the crystallised $LID_{0.5}$:$C5_{0.5}$ was determined by DSC analysis to be approximately 55 °C as shown in **Figure 1A**.

LID:C6 samples analysed were solid and the changes in the diffraction patterns upon increasing LID molar fraction can be observed (**Figure S2f**). The systems of $LID_{0.33}$:$C6_{0.67}$ and $LID_{0.67}$:$C6_{0.33}$ molar compositions display peaks arising from the PXRD patterns of the parent components. In addition to these peaks the formation of a new PXRD pattern is evident. New peaks appearing at lower 2θ in relation to the parent components indicate the formation of a larger crystal lattice. This is observed in all LID:C6 samples with a new peak appearing at 7 2θ degrees. At 1:1 composition only the new PXRD pattern is displayed which most likely signifies the formation of a lidocainium adipate salt. No traces of the parent materials are present at equimolar composition signifying complete conversion. New peaks in the mixtures implied that the intact crystal structures of the parent materials were completely altered via solvent-free mechanosynthesis.

LID:C7 binary mixtures obtained were liquid but contained white particles dispersed within the matrix and attempts to capture the temperature of the melting transition by thermal analysis was

unsuccessful, as explained above. However, it was possible to obtain PXRD pattern of the new phase formed (**Figure S2g**). The existence of a diffraction pattern inferred that the melting point of the new phase must be higher than the room temperature. When subjected to PXRD these particles exhibit a unique PXRD pattern as compared to the parent materials. The new peak at the 7.7 2θ degrees is found at a lower position as compared to the first peaks of the diffraction patterns of the parent components indicating the formation of a larger crystal lattice. The $LID_{0.33}$:$C7_{0.67}$ and $LID_{0.67}$:$C7_{0.33}$ mixtures exhibit PXRD patterns which contain peaks stemming from the parent components in addition to the new peaks. The presence of the parent components within these systems suggests that the material does not participate in the formation of intermolecular interactions and crystallises out as excess. The binary mixture at 1:1 stoichiometry displays only the new peaks attributable to the new phase formed upon mechanical grinding, most likely a 1:1 lidocainium hemipimelate stoichiometry.

PXRD analysis of LID:C8 systems showed similar results as those observed for the LID:C7 system. PXRD patterns with 0.33:0.67 and 0.67:0.33 molar compositions exhibited newly formed peaks as well as peaks characteristic of the parent materials. At the 1:1 stoichiometry no peaks stemming from the precursors were observed indicating 1:1 lidocainium hemisuberate stoichiometry. However, the mixtures at 0.33:0.67 and 0.67:0.33 molar compositions also contain unique peaks not found in other samples (**Figure S2h**, purple dashed boxes). One possible source of these peaks stems from crystallisation of non-stoichiometric phases.

Thermal analysis data was used to construct thermodynamic phase diagrams (**Figure 3**). The theoretical solubility lines were modelled by Schroeder van Laar equation (**Equation 1**):

$$T = \left(\frac{1}{T_{fus}} - \frac{R \ln \chi}{\Delta H_{fus}}\right) \qquad \text{(Eq.1)}$$

where R is the gas constant, χ is the mole fraction of the studied component at a given temperature T; ΔH_{fus} (J mol^{-1}) and T_{fus} denote the enthalpy of fusion and melting temperature of the pure component, respectively. From the phase diagrams obtained it is evident that only LID:C8 phase behaviour could be reasonable predicted. LID:C5 and LID:C7 systems deviate from the ideal behaviour which indicates that additional intermolecular interactions acting between the components in the mixtures contribute to the

thermal events within the systems. Phase diagram obtained for the LID:C6 system shows that the theoretical model cannot be applied in this case as the melting points of the parent components are so far apart that the calculated liquidus lines never converge. In all of the cases the calculated theoretical eutectic composition was not the same as observed in DSC and PXRD studies. The investigation of intermolecular interactions using Fourier transform infrared analysis (FTIR) has confirmed the presence of electrostatic and hydrogen bonding interactions within the systems at various molar compositions. **Table S2** and **Figure S3** highlight the characteristic peaks observed in the FTIR spectra. It is interesting to note that the carbonyl stretch of LID at 1665 cm^{-1} undergoes a hypsochromic shift when mixed with odd DAs and a bathochromic shift when mixed with even DAs. The observed alternation indicates alternating capability of the DAs to form H-bonds with the carbonyl group of LID.

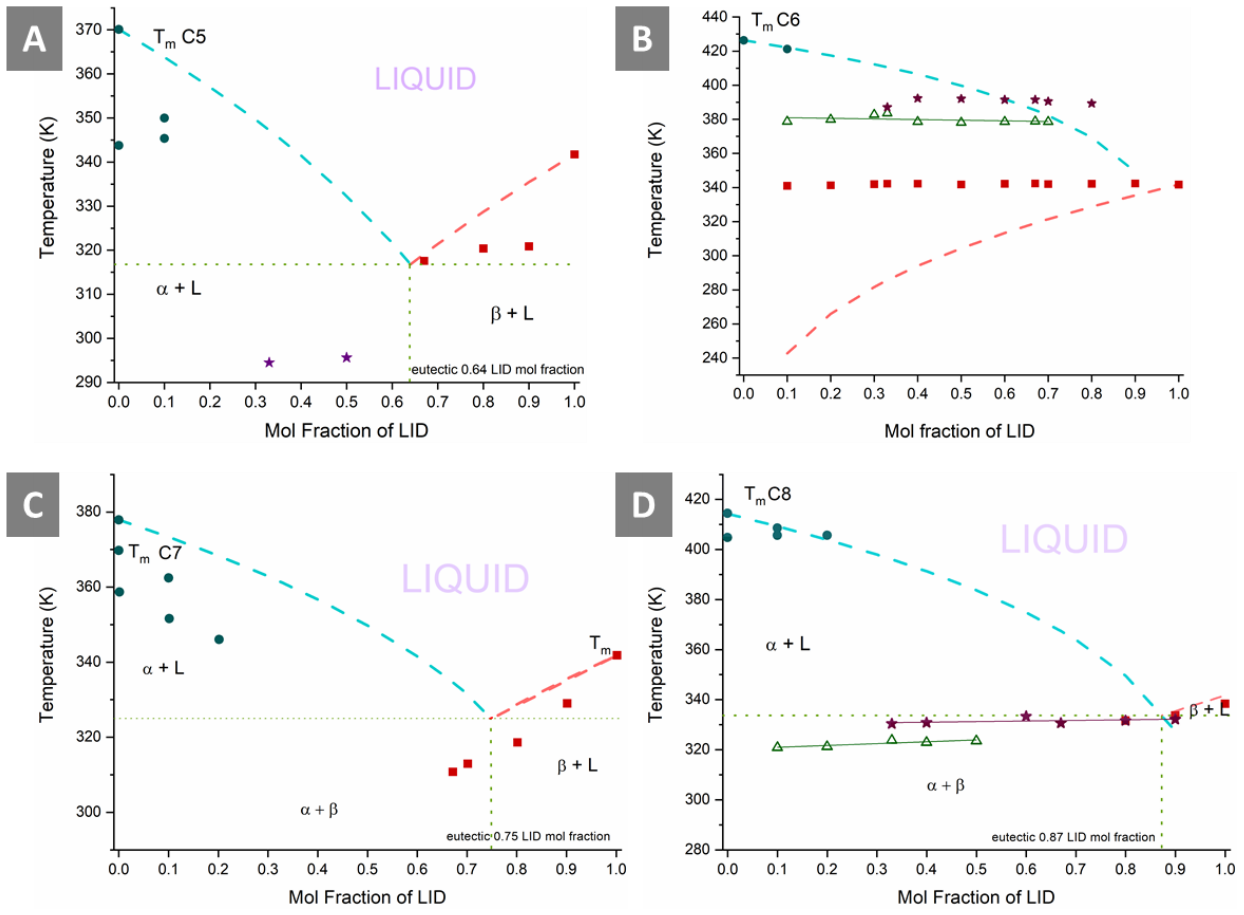

Figure 3. Phase diagrams constructed using the data obtained from DSC experiments. Theoretical curves were constructed using the Schroeder van Laar equation (blue dashed line – theoretical DA solubility curve;

red dashed line - theoretical LID solubility curve). Legend: red squares – experimental LID T_m; green circles - experimental DA T_m; stars - experimental new phase T_m; green triangles - experimental eutectic T_m; α and β indicate diacid and LID components, respectively; L indicates liquefied components.

Thermal and dynamic behaviour of supercooled LID:DA systems

All LID:DAs composition following melting were fast cooled at a nominal rate of 300 K/min and subjected to a second heating cycle at 10 K/min. The stacks of DSC thermograms of the samples at various molar compositions are presented in **Figures S4-S7**. The presence of glass transition (T_g) events in most mixtures (with the exception of extreme molar compositions of LID:C5 and LID:C7) imply the ability of the systems to be supercooled. No glass transition events were observed for the parent materials as they crystallise immediately upon cooling. T_g behaviour of the systems was evaluated and is presented in **Figure 4**.

As can be seen from **Figure 4A**, there is a clear maximum in T_g when the LID:C5 and LID:C7 mixtures are considered. It occurs at the equimolar composition of acid and base. Interestingly, such a trend is not observed for LID:C6 and LID:C8. In the latter case, only the continuous decrease of T_g with the mole fraction of lidocaine can be observed. The peculiar extremum in T_g behaviour found for $LID_{0.5}$:$C5_{0.5}$ and $LID_{0.5}$:$C7_{0.5}$ can be explained in terms of ionicity degree. Typically, the T_g becomes markedly increased when a given API is converted to the salt form e.g. hydrochloride, sulphate or phosphate.[35,36] Additionally, it has been also confirmed that the T_g and melting point of classical aprotic ionic liquids increases when the electrostatic interactions start to dominate van der Waals forces.[37] In this context, one can expect that in LID:C5 and LID:C7 systems there is a proton transport from acid to base, and importantly it is the most efficient in 1-1 compositions. As a consequence, $LID_{0.5}$:$C5_{0.5}$ and $LID_{0.5}$:$C7_{0.5}$ are expected to be composed of LID cations and acidic anions and thus reveal an ionic character.

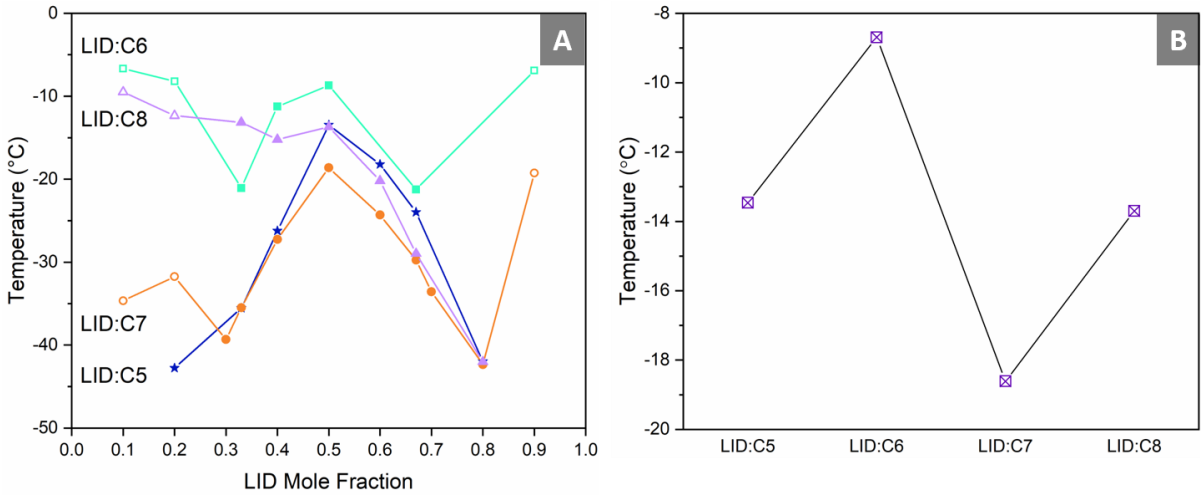

Figure 4. T_g values of the LID:DA systems obtained upon supercooling them in the DSC. (**a**) T_g values of LID:C5 (blue stars), LID:C6 (green squares), LID:C7 (orange circles) and LID:C8 (purple triangles) as a function of LID mole fraction. Open circles denote samples that have partially crystallised upon cooling or during second heating before the T_g was observed; (**b**) T_g values of the systems at equimolar compositions.

The most commonly explored approach for assessing ionicity in ionic liquids is the Walden plot that relates molar conductivity (Λ) of a given system to its viscosity (η), i.e. $\Lambda\eta^{-k}=C$. If the system is composed of independent ions and their diffusion depends only on viscosity then the Walden diagram corresponds closely to the ideal line determined for 0.01 mol dm^{-3} KCl aqueous solution, with the slope equal to 1.[38] Usually, the protic ionic liquids are located below this line on the lower right-hand half of the Walden plot.[39] This is due to the partial ionisation of these systems that results in a lower number of charge carriers and consequently lower conductivity than it would be expected from the Walden rule. For this reason, PILs are frequently regarded as 'poor' ionic systems. However, as demonstrated in the literature, there are examples of superionic protic liquids and glasses that are characterised by the abnormally high mobility of charge-carrying species and fall above the ideal Walden line.[40,41]

To examine the ionicity of LID:C5 and LID:C7 equimolar compositions, conductivity, viscosity and density of these materials need to be determined. Conductivity was measured by dielectric spectroscopy at various temperatures, from 363 K to 243 K for $LID_{0.5}$:$C5_{0.5}$ and from 363K 246 K for $LID_{0.5}$:$C7_{0.5}$. The

representative conductivity spectra $\sigma'(f)$ of $LID_{0.5}$:$C5_{0.5}$ collected in the frequency range from 10^{-1} to 10^{6} Hz are demonstrated in **Figure 5A**.

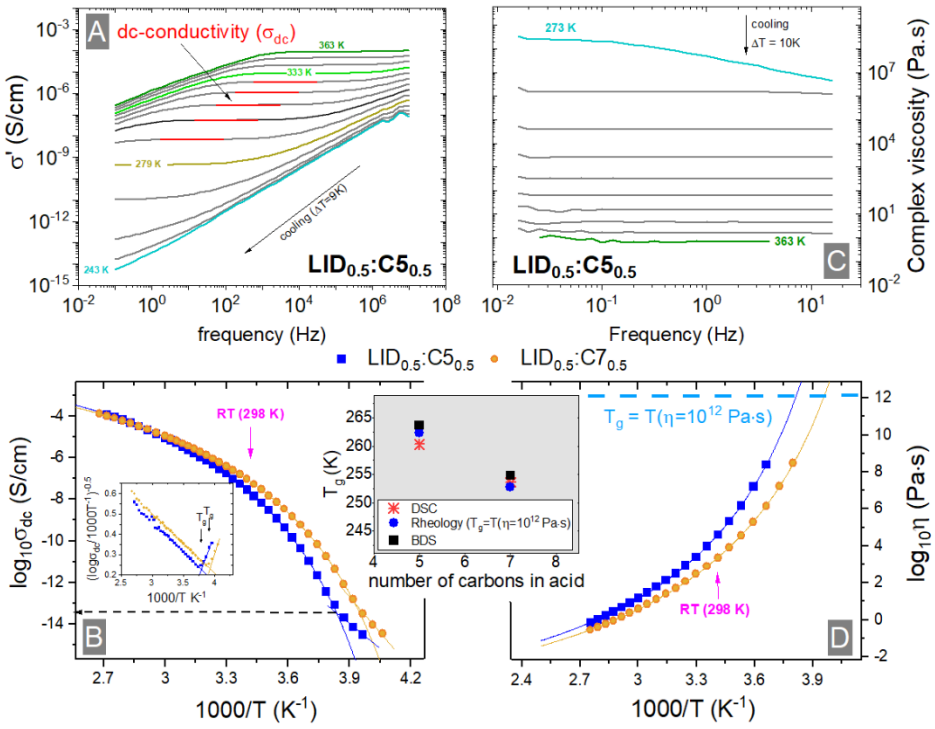

Figure 5. A) Dielectric spectroscopy data of LID:C5 presented in conductivity formalism. B) Temperature dependence of dc-conductivity for $LID_{0.5}$:$C5_{0.5}$ and $LID_{0.5}$:$C7_{0.5}$. The inset presents the Stickel analysis C) Complex viscosity spectra of $LID_{0.5}$:$C5_{0.5}$. D) Temperature dependence of complex viscosity for $LID_{0.5}$:$C5_{0.5}$ and $LID_{0.5}$:$C7_{0.5}$. Solid lines are fits of the Vogel-Fulcher-Tammann equation to the experimental data. In the inset panel the T_g values for $LID_{0.5}$:$C5_{0.5}$ and $LID_{0.5}$:$C7_{0.5}$ determined by conductivity, viscosity and DSC are compared.

Three regions can be detected in the spectra: the polarization effect visible at low frequencies; a frequency-independent part, so-called dc-conductivity, σ_{dc}; and the power-law behaviour at the high frequencies. Since the mobility of ions markedly slows down with cooling, the dc-conductivity also decreases with a decrease in temperature. As shown in **Figure 5B,** the temperature dependence of σ_{dc} reveals a non-linear fashion and can be parameterised by the Vogel-Fulcher-Tammann (VFT) equation (**Equation 2**):

$$\log_{10}\sigma_{\mathrm{dc}}{}^{-1} = \log_{10}\sigma_{\infty}{}^{-1} + \frac{\log_{10}e \cdot DT_0}{T - T_0}, \qquad \text{(Eq. 2)}$$

where σ_{∞}^{-1} is a pre-exponential factor, D is the strength parameter quantifying the deviation from the ideal Arrhenius behaviour and T_0 is known as the "ideal" glass temperature. However, the satisfactory fit to the experimental data can only be achieved in a limited temperature range. This is because below a certain temperature the experimental points follow the Arrhenius behaviour. The VFT-Arrhenius crossover can be better visualised when the Stickel operator $[d\log\tau_{\sigma}/d1000T^{-1}]^{-0.5}$ is employed[42] (inset **Figure 5B**). It should be noted that the crossover phenomenon is a typical feature of ionic glass-formers and it has been proven to define the temperature of liquid-glass transition.[43] This rule is also fulfilled for the studied LID:DA compositions. As seen in the inset to **Figure 5**, the T_g value determined as the crossover point of dc-conductivity data agrees well with the calorimetric T_g. However, upon closer inspection of **Figure 5B** one can also note that dc-conductivity determined at T_g of the LID:DA mixtures is higher than the value of 10^{-15} S/cm typically observed at T_g of classical ionic liquids, in which the vehicle conduction is the only mechanism controlling the charge transport. This result suggests that the fast proton hopping within the Grotthuss conduction gives a contribution to charge transport in the LID:DA compositions. Consequently, viscosity is no longer the main factor controlling charge transport in these systems. To verify this hypothesis, rheological measurements of $LID_{0.5}$:$C5_{0.5}$ and $LID_{0.5}$:$C7_{0.5}$ (**Figures 5C and 5D**) were performed and the conducting and viscoelastic properties of the PILs over a broad temperature range on the Walden plot (**Figure 6**) compared. For the construction of the Walden graph the dc-conductivity needs to be presented as molar conductivity. The following equation was employed for this purpose (**Equation 3**):

$$\Lambda = \sigma_{\mathrm{dc}} \cdot M \cdot \rho^{-1} \qquad \text{(Eq. 3)}$$

where M denotes molecular mass and ρ is density of sample. The molar conductivity data of $LID_{0.5}$:$C5_{0.5}$ and $LID_{0.5}$:$C7_{0.5}$ plotted vs inverse of viscosity in a double-logarithmic scale form a line with the slope k of 0.74 and 0.76, respectively, and importantly, both of them cross the ideal KCl line around room temperature (**Figure 6**). Specifically, $LID_{0.5}$:$C7_{0.5}$ reveals an ideal conductivity at 293 K while $LID_{0.5}$:$C5_{0.5}$ needs to be

heated to 313 K to fall on the ideal line. Additionally, at $T<T_{room}$ both examined PIL fall into the superionic regime, i.e. above the KCl line. A similar behaviour was found for phosphoric acid, an almost ideal proton conductor with confirmed Grotthuss conduction,[44] thus one can conclude that fast proton hopping involving the H-bonding network gives a contribution to charge transport in the LID:DA samples. The proton hopping is the most efficient at low temperatures, i.e. in the vicinity of liquid-glass transition. On the other hand, with increasing temperature, when the mobility of ions becomes faster and H-bonds can be disrupted, the contribution of Grotthuss conduction to the overall charge transport is markedly reduced in $LID_{0.5}$:$C5_{0.5}$ and $LID_{0.5}$:$C7_{0.5}$. The Walden points collected at high temperature can also be used for assessing the ionicity of studied systems. As seen in **Figure 6** at 363 K log $\Lambda(\log\eta^{-1})$ point of $LID_{0.5}$:$C7_{0.5}$ falls on the line denoting 10% of system ionisation. At the same time, $LID_{0.5}$:$C5_{0.5}$ reveals much higher ionisation in the order of 50%. Therefore, it can concluded that the neutral species are active donors in the fast proton conduction process in the examined LID:DA systems.

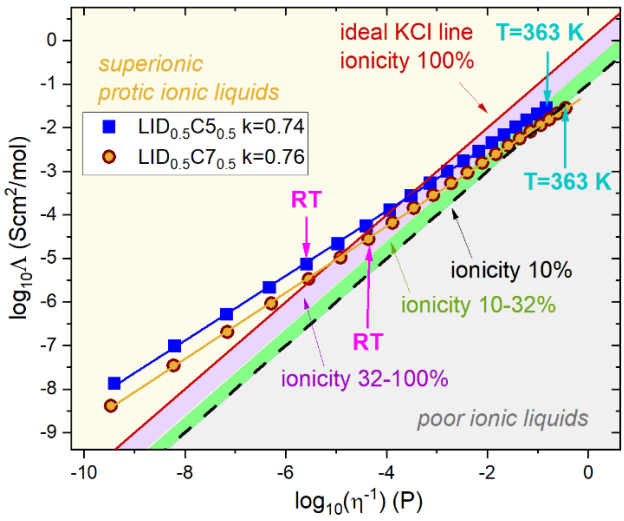

Figure 6. Walden plot of $LID_{0.5}$:$C5_{0.5}$ and $LID_{0.5}$:$C7_{0.5}$.

Crystallographic analysis

The molecular structures of $LID_{0.5}$:$C5_{0.5}$, $LID_{0.5}$:$C6_{0.5}$, $LID_{0.5}$:$C7_{0.5}$ and $LID_{0.5}$:$C8_{0.5}$ are shown in **Figure 7** (details can be found in **Table S3**). The two shorter chain DA molecules crystallise in the

monoclinic system, and the longer chain DA's in the triclinic system. In all structures, the amino group hydrogen and the DA acid hydrogen atoms were located on the difference map and refined with distance restraints. The single deprotonation of the DA is also confirmed by analysis of the bond lengths (*vide infra*) resulting in the corresponding lidocainium hemiglutarate, lidocaininium hemiadipate, lidocaininum hemipimelate and lidocainium hemisuberate salt formation, respectively. Theoretical PXRD patterns generated from the SXRD data closely match experimental PXRD patterns by visual inspection and were fitted using Le Bail Reitveld refinement (**Figures S8-S11**) showing good phase purity in $LID_{0.5}$:$C6_{0.5}$-$LID_{0.5}$:$C8_{0.5}$. $LID_{0.5}$:$C5_{0.5}$ is not phase pure, with poor fitting parameters and shows the incorporation of LID predominately (confirmed by single crystal diffraction).

The asymmetric units of the four complexes, (**Figure 7**), show the 1:1 ratio of LID to DA. In all structures there is a strong hydrogen bond between the amino group in LID and the DA ranging from 2.6118(15) Å in $LID_{0.5}$:$C7_{0.5}$ to 2.6968(11) Å in $LID_{0.5}$:$C6_{0.5}$. Hydrogen bonding between the DA's feature in all the structures (**Figures S12-S15** and **Tables S4-S7**). It is notable that in the C6-C8 extended structures that the DA's align in a chain with head to tail acid hydrogen bonding as a homosynthon. The anionic acid moiety is also hydrogen bonded to the amino group (*vide supra*). There is also weak CH···O hydrogen bonding to both the acidic and anionic DA oxygen atoms. These hydrogen bonding arrangements align the packing into lidocaineH^+:DA stacks, **Figure 7 (E-H)**. However, this regular head to tail DA arrangement is not observed in the C5 structure. In this case, the DA's are aligned in a staggered side-to-side hydrogen bonding homosynthon. This is assisted with strong amino hydrogen bonding to the anionic acid end and weaker C-H···O hydrogen bonding (chelate forming) to the carboxylic acid C5 moiety.

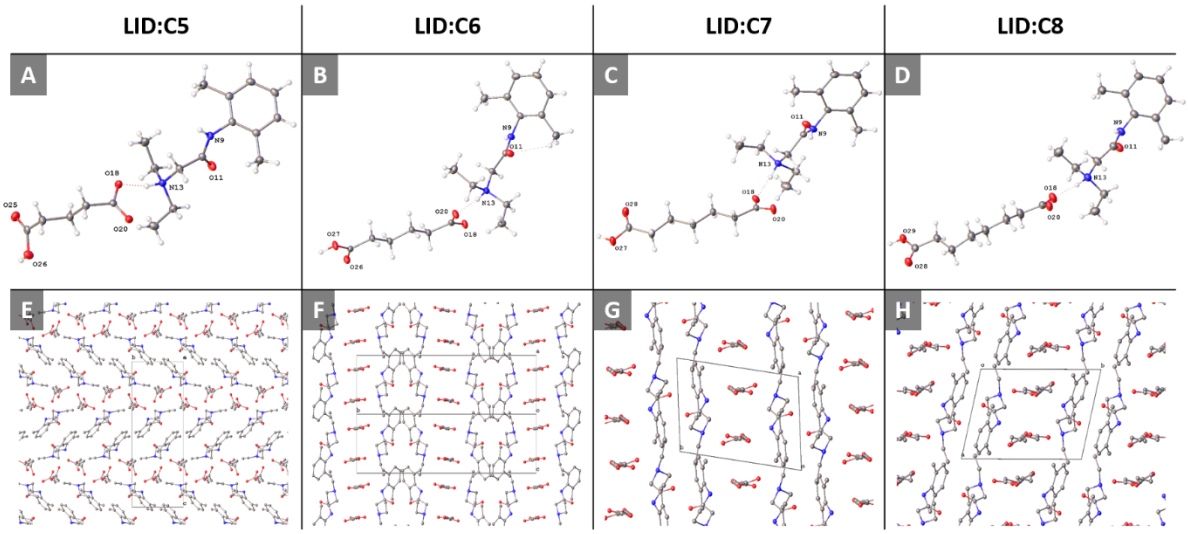

Figure 7. Molecular structures of the ion pairs (**A**) LID:C5 (**B**) LID:C6 (**C**) LID:C7 and (**D**) LID:C8 with heteroatoms labelled only and atomic displacement shown at 50% probability. Red dotted lines show hydrogen bonding from LID to the DA. Packing diagrams of (**E**) LID:C5 viewed normal to (100) showing the staggered DA homosynthon, (**F**) LID:C6 viewed normal to (101), (**D**) LID:C7 viewed normal to (001) and (**H**) LID:C8 viewed normal to (001) with linear homosynthons. All are viewed perpendicular to the stack direction and hydrogen atoms omitted for clarity.

The evidence for N(13)-H(13) ionic bond formation is deduced from the carboxylic acid C-O bond lengths ($D_{C\text{-}O}$). It has been shown that in complexes where carboxylic acid deprotonation takes place the resulting carboxylate ion possesses two C-O bonds with similar $D_{C\text{-}O}$, i.e. the $\Delta D_{C\text{-}O} < 0.03$ Å, where $\Delta D_{C\text{-}O}$ is the difference in length between the two C-O bonds within a carboxylate moiety. On the other end of the ionisation spectrum, neutral carboxylic acids would possess two distinct C-O bonds with $\Delta D_{C\text{-}O} > 0.08$ Å.[45] The $\Delta D_{C\text{-}O}$ values obtained for all 4 complexes were ≤ 0.04 Å indicating carboxylate ion formation (**Table S8**). The calculated values correlate well with expected salt formation based on ΔpK_a between an acid and a base (i.e. salt formation is expected if $\Delta pK_a > 3$).[46]

Crystal structure and crystal packing profoundly affect the molecular-loosening and molecular-change steps of a solid state reaction.[47,48] The influence of crystal packing on solid-state reactivity is described by topochemical postulates. It is generally accepted that a reaction is topochemical if the structure of the product can be explained by the crystal packing of the reactant crystal.[47] Crystal voids were calculated

in an attempt to correlate crystal packing efficiency to the observed melting point variation. It has been shown previously that ratios of volume occupied by molecules to unit cell, known as Kitaigorodskii Packing Indices (KPIs)[49], allow to compare packing efficiency and predict the T_m of the solid. However, opposite crystal packing effects have also been recognised.[25] **Table S9** reveals that the predicted trend is not followed in the parent DAs. Therefore, the efficiency of the crystal packing of the parent components is not the main determinant of the T_m and crystal packing trends in the salt products. However, an alternating trend was observed in the KPI values of the LID:DA systems which corroborates their crystallisation tendencies. The systems with lower KPIs and greater void spaces were slow-crystallisation systems that tend to stay liquid at room temperature.

The effect of salt formation on the molecular conformations of each molecule within the complexes was investigated. Molecular overlays of the experimental and reference crystal structures were calculated and the similarity is expressed in terms of Root-Mean-Square-Deviation (RMSD) values, where large RMSD values indicate greater differences between the molecules. LID molecules from the LID:DA single crystals were overlaid with reference LID structure (CSD ID LIDCAN11), however, no obvious trends were discerned. Furthermore, Hirshfeld analysis of LID within the new salt complexes have not revealed significant variations that could explain the alternation in physicochemical properties of the systems. The only notable difference is the diffuse blue regions observed in $LID_{0.5}$:$C6_{0.5}$ and $LID_{0.5}$:$C8_{0.5}$ crystals as seen in **Figure S16**. This region suggests that a part of a molecular surface has large distances to the nearest atoms which is generally characteristic of less than ideal packing arrangement.[50] The breakdown of the close-contact intermolecular contributions to the Hirshfeld surface area display no significant variation for the four salt complexes as seen in **Figure S16I**.

Figure 8 present overlays of reference parent DA structures (CSD ID: HITSAG, ADIPAC14, PIMELA08, SUBRAC06) with ionised DA structures obtained from SXRD data. It is interesting to observe that the longer is the DA chain, the greater is the RMSD value. It appears that DAs undergo conformational changes in order to adapt to the length of the LID molecule in order to form the required number of crystal-stabilising hydrogen bonds. However, $LID_{0.5}$:$C5_{0.5}$ does not follow this trend. This exception is consistent

with the different crystal packing of this system. The carboxyl moieties are rotated in order to form both carboxyl - carboxyl H-bonds with another single C5 molecule (O(26)-H(26)···O(18), symmetry operation-x+2,y-1/2,-z+1/2). As a result, this system lacks the ribbon-like crystal packing found in the rest of the series.

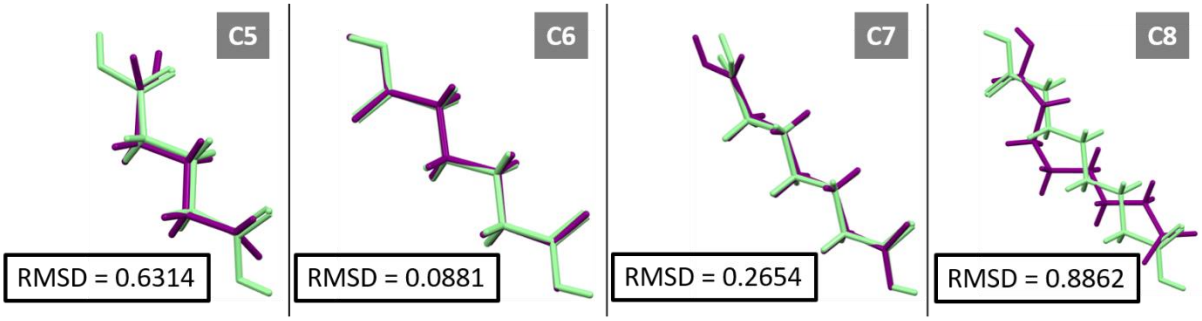

Figure 8. Molecular overlay of C6 - ADIPAC08 (green) with $LID_{0.5}$:$C6_{0.5}$ (purple); C7 - PIMELA06 (green) with $LID_{0.5}$:$C7_{0.5}$ (purple); C8 - SUBRAC05 (green) with $LID_{0.5}$:$C8_{0.5}$ (purple). Corresponding Root-Mean-Square-Deviation (RMSD) values for the overlays are presented in boxes.

Conclusions

Lidocainium hemiadipate solid salt and lidocainium hemiglutarate, lidocainium hemipimelate, lidocainium hemsuberate ILs were successfully prepared by a simple mechanochemical solvent-free grinding. The thermal and ionisation behaviour of the systems have been investigated in detail. Upon examination of the trends in physicochemical properties it was found that the even-odd melting point alternation of DAs is generally retained in LID:DA complexes. In-depth investigation into the crystallographic properties of the DAs and the synthesised salts provided some explanations on the alternating variability of the physicochemical properties among the series. This study brought us closer to understanding the mechanisms of ILs formation and contributed to the current aim of the ILs community to devise a systematic approach for IL discovery and development.

Associated Content

Supporting Information

The Supporting Information is available free of charge at https://pubs.acs.org . The file contains: Experimental Section, Thermal Analysis (First Heating) and Powder X-ray Diffraction, Infrared Analysis, Thermal Analysis (Second Heating), Crystallographic Analysis and Hydrogen Bonding Motifs sections.

Author Information

Corresponding Author

Lidia Tajber - School of Pharmacy and Pharmaceutical Sciences, Trinity College Dublin, College Green, Dublin 2, Ireland. ORCID 0000-0003-1544-6796, email: ltajber@tcd.ie

Authors

Julija Zotova - School of Pharmacy and Pharmaceutical Sciences, Trinity College Dublin, College Green, Dublin 2, Ireland, email: zotovaj@tcd.ie

Zaneta Wojnarowska - Institute of Physics, University of Silesia, SMCEBI, 75 Pulku Piechoty 1A, 41-500 Chorzow, Poland. ORCID 0000-0002-7790-2999, email: zaneta.wojnarowska@smcebi.edu.pl

Brendan Twamley - School of Chemistry, Trinity College Dublin, College Green, Dublin 2, Ireland, email: twamleyb@tcd.ie

Marian Paluch - Institute of Physics, University of Silesia, SMCEBI, 75 Pulku Piechoty 1A, 41-500 Chorzow, Poland. ORCID 0000-0002-7280-8557, email: marian.paluch@us.edu.pl

Author Contributions

The manuscript was written through contributions of all authors. All authors have given approval to the final version of the manuscript.

Funding Sources

This research was funded by Science Foundation Ireland, grant number 15/CDA/3602. Z.W. and M.P. are grateful for the financial support by the National Science Centre within the framework of the Symfonia3

project Grant No. DEC2015/16/W/NZ7/00404. The authors would like to acknowledge COST Action CA18112 “Mechanochemistry for Sustainable Industry”.

Notes

The authors declare no competing financial interest.

References

(1) Domingos, S.; André, V.; Quaresma, S.; Martins, I. C. B.; Minas Da Piedade, M. F.; Duarte, M. T. New Forms of Old Drugs: Improving without Changing. *J. Pharm. Pharmacol.* **2015**, *67* (6), 830–846.

(2) Braga, D.; Grepioni, F.; Maini, L. The Growing World of Crystal Forms. *Chem. Commun.Commun.* **2010**, *46*, 6232–6242.

(3) Berry, D. J.; Steed, J. W. Pharmaceutical Cocrystals, Salts and Multicomponent Systems; Intermolecular Interactions and Property Based Design. *Adv. Drug Deliv. Rev.* **2017**, *117*, 3–24.

(4) Stahl, P. H.; Wermuth, C. G. *Handbook of Pharmaceutical Salts : Properties, Selection, and Use*, 2nd ed.; Wiley-VCH, VHCA: Weinheim, Zurich, 2011.

(5) Rogers, R. D.; Seddon, K. R. Ionic Liquids - Solvents of the Future? *Science (80-.).* **2003**, *302* (5646), 792–793.

(6) Hough, W. L.; Smiglak, M.; Rodríguez, H.; Swatloski, R. P.; Spear, S. K.; Daly, D. T.; Pernak, J.; Grisel, J. E.; Carliss, R. D.; Soutullo, M. D.; et al. The Third Evolution of Ionic Liquids: Active Pharmaceutical Ingredients. *New J. Chem.* **2007**, *31* (8), 1429.

(7) Shamshina, J. L.; Barber, P. S.; Rogers, R. D. Ionic Liquids in Drug Delivery. *Expert Opin. Drug Deliv.* **2013**, *10* (10), 1367–1381.

(8) Mccrary, P. D.; Beasley, P. A.; Gurau, G.; Narita, A.; Barber, P. S.; Cojocaru, O. A.; Rogers, R. D. Drug Specific, Tuning of an Ionic Liquid's Hydrophilic–Lipophilic Balance to Improve Water Solubility of Poorly Soluble Active Pharmaceutical Ingredients. *New J. Chem.* **2196**, *37* (37), 2196–2202.

(9) Tan, D.; Loots, L.; Friščić, T. Towards Medicinal Mechanochemistry: Evolution of Milling from Pharmaceutical Solid Form Screening to the Synthesis of Active Pharmaceutical Ingredients (APIs). *Chem. Commun.* **2016**, *52*, 7760–7781.

(10) Karimi-Jafari, M.; Padrela, L.; Walker, G. M.; Croker, D. M. Creating Cocrystals: A Review of Pharmaceutical Cocrystal Preparation Routes and Applications. *Cryst. Growth Des.* **2018**, *18* (10), 6370–6387.

(11) Martins, I. C. B.; Oliveira, M. C.; Diogo, H. P.; Branco, L. C.; Duarte, M. T. MechanoAPI-ILs: Pharmaceutical Ionic Liquids Obtained through Mechanochemical Synthesis. *ChemSusChem*

2017, *10* (7), 1360–1363.

(12) Earle, M. J.; Seddon, K. R. Ionic Liquids. Green Solvents for the Future. *Pure Appl. Chem.* **2000**, *72* (7), 1391–1398.

(13) Crawford, D. E.; Porcheddu, A.; McCalmont, A. S.; Delogu, F.; James, S. L.; Colacino, E. Solvent-Free, Continuous Synthesis of Hydrazone-Based Active Pharmaceutical Ingredients by Twin-Screw Extrusion. *ACS Sustain. Chem. Eng.* **2020**, *8* (32), 12230–12238.

(14) Dean, P. M.; Pringle, J. M.; MacFarlane, D. R. Structural Analysis of Low Melting Organic Salts: Perspectives on Ionic Liquids. *Phys. Chem. Chem. Phys.* **2010**, *12* (32), 9144–9153.

(15) Krossing, I.; Slattery, J. M.; Daguenet, C.; Dyson, P. J.; Oleinikova, A.; Weingärtner, H. Why Are Ionic Liquids Liquid? A Simple Explanation Based on Lattice and Solvation Energies. *J. Am. Chem. Soc.* **2006**, *128* (41), 13427–13434.

(16) Manin, A. N.; Drozd, K. V; Churakov, A. V; Perlovich, G. L.; Krestov, G. A. Hydrogen Bond Donor/Acceptor Ratios of the Coformers: Do They Really Matter for the Prediction of Molecular Packing in Cocrystals? The Case of Benzamide Derivatives with Dicarboxylic Acids. *Cryst. Growth Des.* **2018**, *18* (9), 5254–5269.

(17) Turanjanin, J.; Scott, J. L.; MacFarlane, D. R.; Yoshizawa-Fujita, M.; Dean, P. M. Exploring an Anti-Crystal Engineering Approach to the Preparation of Pharmaceutically Active Ionic Liquids. *Cryst. Growth Des.* **2008**, *9* (2), 1137–1145.

(18) Umerska, A.; Bialek, K.; Zotova, J.; Skotnicki, M.; Tajber, L. Anticrystal Engineering of Ketoprofen and Ester Local Anesthetics: Ionic Liquids or Deep Eutectic Mixtures? *Pharmaceutics* **2020**, *12* (4), 368.

(19) Sedef Gocmen, J.; Buyukkocak, U.; Caglayan, O.; Aksoy, A. In Vitro Antibacterial Effects of Topical Local Anesthetics. *J. Dermatolog. Treat.* **2008**, *19* (6), 351–353.

(20) Pina-Vaz, C.; Rodrigues, A. G.; Sansonetty, F.; Martinez-De-Oliveira, J.; Fonseca, A. F.; Mårdh, P.-A. Antifungal Activity of Local Anesthetics Against Candida Species. *Infect. Dis. Obstet. Gynecol.* **2000**, *8* (3–4), 124–137.

(21) Pérez-Isidoro, R.; Sierra-Valdez, F. J.; Ruiz-Suárez, J. C. Anesthetic Diffusion Through Lipid Membranes Depends on the Protonation Rate. *Sci. Rep.* **2015**, *4* (1), 7534.

(22) Martin, H.; Maris, P. Synergism between Hydrogen Peroxide and Seventeen Acids against Six

Bacterial Strains. *J.Appl.Microbiol.* **2012**, *113* (3), 578–590.

(23) Braga, D.; Chelazzi, L.; Grepioni, F.; Dichiarante, E.; Chierotti, M. R.; Gobetto, R. Molecular Salts of Anesthetic Lidocaine with Dicarboxylic Acids: Solid-State Properties and a Combined Structural and Spectroscopic Study. *Cryst. Growth Des.* **2013**, *13* (6), 2564–2572.

(24) Berton, P.; Kelley, S. P.; Wang, H.; Rogers, R. D. Elucidating the Triethylammonium Acetate System: Is It Molecular or Is It Ionic? *J. Mol. Liq.* **2018**, *269*, 126–131.

(25) Bhattacharya, S.; Saraswatula, V. G.; Saha, B. K. Thermal Expansion in Alkane Diacids - Another Property Showing Alternation in an Odd-Even Series. *Cryst. Growth Des.* **2013**, *13* (8), 3651–3656.

(26) Thalladi, V. R.; Nu, M.; Boese, R. The Melting Point Alternation in R,ω-Alkanedicarboxylic Acids. *J. Am. Chem. Soc.* **2000**, *122* (38), 9227–9236.

(27) Mishra, M. K.; Ramamurty, U.; Desiraju, G. R. Hardness Alternation in α,ω-Alkanedicarboxylic Acids. *Chem. - An Asian J.* **2015**, *10* (10), 2176–2181.

(28) Lindemann, F. A. Ueber Die Berechnung Molekularer Eigenfrequenzen. *Phys. Z.* **1910**, No. 11, 609–612.

(29) Tothadi, S.; Sanphui, P.; Desiraju, G. R. Obtaining Synthon Modularity in Ternary Cocrystals with Hydrogen Bonds and Halogen Bonds. *Cryst. Growth Des.* **2014**, *14* (10), 5293–5302.

(30) Tothadi, S.; Desiraju, G. R. Synthon Modularity in 4-Hydroxybenzamide−Dicarboxylic Acid Cocrystals. *Cryst. Growth Des.* **2012**, *12* (12), 6188–6198.

(31) Neville, G. A.; Regnier, Z. R. Hydrogen Bonding in Lidocaine Salts. I. The NH Stretching Band and Its Dependence on the Associated Anion. *Can. J. Chem.* **1969**, *47*, 4229–4235.

(32) Bica, K.; Shamshina, J.; Hough, W. L.; MacFarlane, D. R.; Rogers, R. D. Liquid Forms of Pharmaceutical Co-Crystals: Exploring the Boundaries of Salt Formation. *Chem. Commun.* **2011**, *47* (8), 2267–2269.

(33) Ganguly, S.; Ramachandra Rao, C.; Ramachandra Swamy, H. Vibrational Spectroscopic Studies of Phase Transitions in Organic Molecular Crystals and Dicarboxylic Acids. *Croat. Chem. Acta* **1982**, *55* (1–2), 207–221.

(34) Jagannathan, N. R.; Rao, C. N. R. A 13C NMR Spectroscopic Study of the Phase Transitions of Alkane Dicarboxylic Acids in the Solid State. *Chem. Phys. Lett.* **1987**, *140* (1), 46–50.

(35) Kaminski, K.; Kaminska, E.; Adrjanowicz, K.; Grzybowiska, K.; Wlodarczyk, P.; Paluch, M.; Burian, A.; Ziolo, J.; Lepek, P.; Mazgalski, J.; et al. Dielectric Relaxation Study on Tramadol Monohydrate and Its Hydrochloride Salt. *J. Pharm. Sci.* **2010**, *99* (1), 94–106.

(36) Stoimenovski, J.; Dean, P. M.; Izgorodina, E. I.; MacFarlane, D. R. Protic Pharmaceuticalionic Liquids and Solids: Aspects of Protonics. *Faraday Discuss.* **2012**, *154*, 335–352.

(37) Sippel, P.; Lunkenheimer, P.; Krohns, S.; Thoms, E.; Loidl, A. Importance of Liquid Fragility for Energy Applications of Ionic Liquids. *Sci. Rep.* **2015**, *5* (1), 1–8.

(38) *Electrochemical Aspects of Ionic Liquids*; Ohno, H., Ed.; Wiley: New Jersey, 2005.

(39) Angell, C. A.; Byrne, N.; Belieres, J. P. Parallel Developments in Aprotic and Protic Ionic Liquids: Physical Chemistry and Applications. *Acc. Chem. Res.* **2007**, *40* (11), 1228–1236.

(40) Wojnarowska, Z.; Wang, Y.; Pionteck, J.; Grzybowska, K.; Sokolov, A. P.; Paluch, M. High Pressure as a Key Factor to Identify the Conductivity Mechanism in Protic Ionic Liquids. *Phys. Rev. Lett.* **2013**, *111* (22), 225703.

(41) Wojnarowska, Z.; Wang, Y.; Paluch, K. J.; Sokolov, A. P.; Paluch, M. Observation of Highly Decoupled Conductivity in Protic Ionic Conductors. *Phys. Chem. Chem. Phys.* **2014**, *16* (19), 9123–9127.

(42) Stickel, F.; Fischer, E. W.; Richert, R. Dynamics of Glass-Forming Liquids. II. Detailed Comparison of Dielectric Relaxation, de-Conductivity, and Viscosity Data. *J. Chem. Phys.* **1996**, *104* (5), 2043–2055.

(43) Wojnarowska, Z.; Paluch, M. Recent Progress on Dielectric Properties of Protic Ionic Liquids. *J. Phys. Condens. Matter* **2015**, *27* (7), 073202.

(44) Dippel, T.; Kreuer, K. D.; Lassègues, J. C.; Rodriguez, D. Proton Conductivity in Fused Phosphoric Acid; A 1H/31P PFG-NMR and QNS Study. *Solid State Ionics* **1993**, *61* (1–3), 41–46.

(45) Childs, S. L.; Stahly, G. P.; Park, A. The Salt-Cocrystal Continuum: The Influence of Crystal Structure on Ionization State. *Mol. Pharm.* **2007**, *4* (3), 323–338.

(46) Stoimenovski, J.; Izgorodina, E. I.; MacFarlane, D. R. Ionicity and Proton Transfer in Protic Ionic Liquids. *Phys. Chem. Chem. Phys.* **2010**, *12* (35), 10341–10347.

(47) Singh, N. B.; Singh, R. J.; Singh, N. P. Organic Solid State Reactivity. *Tetrahedron* **1994**, *50* (22), 6441–6493.

(48) Paul, I. C.; Curtin, D. Y. Thermally Induced Organic Reactions in the Solid State. *Acc. Chem. Res.* **1973**, *6* (7), 217–225.

(49) Kitaigorodskii, A. I. *Molecular Crystals and Molecules*; Academic Press: New York, 1973.

(50) McKinnon, J. J.; Spackman, M. A.; Mitchell, A. S. Novel Tools for Visualizing and Exploring Intermolecular Interactions in Molecular Crystals. *Acta Crystallogr. Sect. B Struct. Sci.* **2004**, *60* (6), 627–668.